https://doi.org/10.5194/egusphere-2026-1141
Preprint. Discussion started: 25 March 2026

Enhanced removal of very low frequency (VLF) and low frequency (LF) radio noise from transient electromagnetic (TEM) data with modeling and adaptive filtering

Michel Hardenberg[1] and Jakob Juul Larsen[1]

[1]Department of Electrical and Computer Engineering, Aarhus University, Finlandsgade 22, 8200 Aarhus N, Denmark

Correspondence: Jakob Juul Larsen (jjl@ece.au.dk)

Abstract. Interference from very low frequency (VLF, 3-30 kHz) and low frequency (LF, 30-300 kHz) radio stations is a ubiquitous and challenging noise source in transient electromagnetic (TEM) data. It can be difficult to suppress interfering radio signals with the commonly applied methods of gating and stacking. However, the characteristics of VLF and LF radio signals encoded with minimum-shift keying methods allow for a better solution where the noise is modeled and subtracted. This approach has previously been shown to give good results for continuous streams of TEM data. Recently proposed new use cases for TEM instrumentation, such as time-lapse measurements of fluctuating groundwater levels and dynamic groundwater-saltwater interfaces produce discontinuous streams of TEM data with regular gaps between individual transients. We show that under mild constraints of data availability, radio signals can still be modeled in this case. We further show that the addition of an adaptive filter can fine-tune the radio model and improve the signal-to-noise ratio. The performance is analyzed on a synthetic noise data set and on a real field noise data set. For this field noise data set, we find that the standard errors of early time TEM data are improved by about a factor of two.

1 Introduction

Transient electromagnetics (TEM) is a widely used geophysical method for, e.g., mineral exploration (Gisselø et al., 2024), hydrogeophysical investigations (Behroozmand et al., 2019; Chandra et al., 2019), and geotechnical applications (Lysdahl et al., 2022; With et al., 2022). The method is versatile and both ground based and airborne instruments are common. The ability to use instruments on mobile platforms provides the means for dense spatial coverage and large-scale airborne mappings with thousands of line kilometers are today standard operations. The TEM method is continuously being developed, and active research topics include instruments carried by unmanned aerial vehicles (Qi et al., 2020), inversion of data sets of ever-increasing size (Engebretsen et al., 2022), and the incorporation of machine learning algorithms in processing and inversion of TEM data (Wu et al., 2022; Asif et al., 2022).

The main feature of TEM is mapping of resistivity structures in the subsurface, but repeated measurements at the same site can be used to track temporal changes in the sub-surface. One early example of such time-lapse TEM was an attempt to track changes in a French underground gas storage site (Hördt et al., 2000). Unfortunately, no changes could be detected due to insufficient signal-to-noise ratio and instabilities in the transmitter pulses. Other more successful examples include the

https://doi.org/10.5194/egusphere-2026-1141
Preprint. Discussion started: 25 March 2026

monitoring of changes in the TEM response caused by artificial infiltration (Swidinsky and El-Kaliouby, 2013) or caused by a pumping test (Chen et al., 2019).

One common feature of these examples is small data sets consisting of a few measurements done before and after an event. A different use-case of time-lapse TEM has recently been suggested by Zamora-Luria et al. (2023). Here, the goal is to continuously track changes in groundwater levels or in groundwater-salt water interfaces obtained by observing dynamic changes in the resistivity model of the subsurface. Experimentally, this is achieved by installing a remotely operated TEM instrument with transmitter and receiver coils buried below the surface at a site and having the instrument autonomously conduct one or several daily measurements.

Time-lapse TEM is attempting to detect the changes in resistivity caused by, e.g., a groundwater level change by a few tens of cm. However, the changes are minuscule and embedded in the fixed resistivity structure from the geological background, which makes them difficult to discern. Data sets with very high signal-to-noise ratios are therefore crucial.

Signals from very low frequency (VLF, 3-30 kHz) and low frequency (LF, 30-300 kHz) long range communication radio stations are commonly used as a low-cost geophysical prospecting method (Eppelbaum, 2021) but for TEM data collection, these radio signals are a troublesome source of noise (Macnae, 2015; McLachlan et al., 2023). A particularity of this radio noise is that it in unlucky cases, it can act as a coherent noise source where the radio signal and the repeating TEM signal are accidentally in phase. If so, the standard stacking of multiple TEM measurements to reduce noise will not cancel the radio signal from data but instead lead to a biased TEM signal with low standard deviation (Larsen et al., 2021).

The VLF and LF radio noise can be suppressed by gating the recorded TEM signals with tapered or semi-tapered gates with optimized frequency responses (Larsen et al., 2021; Peng et al., 2022; Khare et al., 2024). However, gating cannot completely remove the radio noise. Further, gating is a low-pass filter operation, and it is therefore only effective in the gates where there is a spectral separation between the TEM signal and the radio noise.

A potentially better approach to handling the radio noise is based on the well-defined structure of most radio signal. These are typically 200 bits/second data streams encoded using minimum-shift keying (MSK). By decoding the radio signals and estimating signal parameters it is possible to model and subtract the radio noise as demonstrated by Macnae (2015) and later improved upon with the use of a more robust decoding technique by Rasmussen et al. (2018).

In this paper we revisit the model-and-subtract approach motivated by the need for very high signal-to-noise ratio time-lapse TEM data (Zamora-Luria et al., 2023). First, we show that the algorithms used in Rasmussen et al. (2018) for estimating symbol timing and phase of the minimum-shift keying encoded radio signals can be lacking in accuracy and that performance can be improved by adding an adaptive filter for fine tuning. Further, the model-and-subtract workflow was originally designed for airborne TEM, where the receiver coil is put in the zero position of the transmitter coil (Rasmussen et al., 2018). The zero positioning minimizes the coupling of the primary field from the transmitter coil into the receiver coil. This makes it possible to cancel the primary field and data processing can be done on long uninterrupted time series. However, zero-positioning is not possible in our use-case with a different transmitter-receiver coil layout, and the strong primary field prohibits recording of data during the transmitter pulses (Zamora-Luria et al., 2023). This leaves large, regularly spaced gaps in data streams.

https://doi.org/10.5194/egusphere-2026-1141
Preprint. Discussion started: 25 March 2026

Consequently, we alter and optimize the data processing to handle these gaps in data. Finally, we analyze the increase in data fidelity obtained with VLF modeling and subtraction compared to only semi-tapered gating.

The outline of this paper is as follows. The following section gives a brief background of transient electromagnetics and commonly encountered noise, in particular MSK-encoded radio noise. This is followed by a methods section detailing our processing steps. In the results sections we demonstrate the performance using both synthetic and real data. This is followed by a discussion and concluding remarks.

2 Background

2.1 Transient electromagnetics

For a full description of transient electromagnetics, we refer to one of the many excellent expositions in the literature, e.g., Nabighian and Macnae (1991). Briefly, a TEM measurement is carried out by applying an input current pulse to a transmitter coil, ground based or airborne. The flow of current generates a primary magnetic field, which penetrates the ground. The transmitter current is abruptly turned off, which induces eddy currents in the ground. The eddy currents give rise to a secondary magnetic field which is measured with a receiver coil. One single measurement is denoted as a transient, and multiple transients are stacked (averaged) into a sounding curve. The decay of the secondary magnetic field is controlled by subsurface resistivity, which can therefore be inferred by modeling of data.

2.2 Noise in transient electromagnetics data

Receiver coils used for TEM measurements are typically designed for wide bandwidth operation (>100 kHz) to enable data acquisition as soon as possible after the turn-off of the transmitter pulse. Most of the noise found in TEM data is external noise inductively coupled into the receiver coil. This includes electromagnetic interference from powerlines and electrical infrastructure, interference from radio stations in the very low frequency (VLF), 3 kHz to 30 kHz, and low frequency (LF) 30 kHz to 300 kHz bands, and interference from natural sources such as thunderstorms. Further, TEM data also contains thermal noise from the receiver coil and the amplifier electronic circuits.

Different methods are used to suppress individual noise sources. As an example, powerline noise can be efficiently removed by synchronous detection (Macnae et al., 1984). This consists of transmitting current pulses of alternating polarity at the powerline fundamental frequency, i.e., 50 Hz or 60 Hz, followed by a sign correction and stacking of data.

2.3 Minimum-shift keying

Many radio stations in the VLF and LF ranges employ encoding with minimum-shift keying. This is a digital format where the bit stream, $s(t)$ is encoded using two different frequencies, f_0 and f_1, with frequency difference $\Delta f = f_1 - f_0$ and center frequency $f_c = (f_0 + f_1)/2$, (Rasmussen et al., 2018). Each bit, normally denoted as a symbol, has a duration T_{sym} with

https://doi.org/10.5194/egusphere-2026-1141
Preprint. Discussion started: 25 March 2026

$\Delta f = 0.5/T_{sym}$. In practice, four symbols are used

$$s_0(t) = \cos\big((2\pi(f_c - \Delta f/2)t\big), \quad \bar{s}_0(t) = -s_0(t)$$
$$s_1(t) = \cos\big((2\pi(f_c + \Delta f/2)t\big), \quad \bar{s}_1(t) = -s_1(t) \tag{1}$$

where the negative sign symbols are used to ensure phase continuity of the signal. The enforcement of phase continuity gives a correlation between adjacent bits which enables efficient decoding of bit streams (Rasmussen et al., 2018).

3 Methods

3.1 Radio signal modeling and subtraction

The radio signal modeling and subtraction approach contains four steps (Rasmussen et al., 2018).

1. Estimation and correction of signal parameters using the acquired data.
2. Estimation of the bit stream from the corrected data.
3. Reconstruction of a clean radio signal from the bit stream and the estimated signal parameters.
4. Subtracting the reconstructed radio signal from the acquired data.

An acquired data set will typically contain interference from multiple VLF and LF radio stations operating at different frequencies and the four steps are repeated sequentially for each radio station signal. Here, we briefly discuss the contents of each step shown in Fig. 1. For a full description, we refer to Rasmussen et al. (2018).

Two main differences to this prior work are first that our data streams are not continuous but interrupted by regular gaps, which can potentially throw the estimation algorithms off and second that an adaptive filter is introduced as a final step to improve the reconstruction.

For each radio signal, the first step of the processing is a down-conversion of the signal to base band by multiplication with a complex exponential at the center frequency, f_c, followed by low-pass filtering to pick out the radio signal of interest. An important design criterion is that the bandwidth of the low-pass filter should be narrow enough to filter out other radio stations and noise sources from the base band signal. However, the high sample rate of around 0.5-4 MHz in full-sampled TEM data implies that the impulse response of the low-pass filter becomes very long. We use a fifth-order Butterworth filter with a cut-off frequency of 100 Hz or 200 Hz according to the bit rate of the specific radio signal and the impulse response can last for more than 10 ms. In our case where the typical time between transmitter pulse is around 1 ms, the impulse response therefore spans multiple segments of data and gaps, and significant transient distortion is introduced at the transitions between data and gaps.

The next processing step is an estimation of three signal parameters, symbol transition time or symbol timing, $\tau \in [-T_{sym}/2, T_{sym}/2]$, signal phase, $\theta \in [0, 2\pi]$, and signal amplitude. Symbol timing and phase are estimated with the algorithms developed by Morelli and Vitetta (1999). The amplitude is estimated by integrating the signal over a 1 s time record and normalizing to the size of the gaps. Following correction for symbol timing and phase we use a Viterbi decoder to estimate the bit stream $B[m]$.

https://doi.org/10.5194/egusphere-2026-1141
Preprint. Discussion started: 25 March 2026

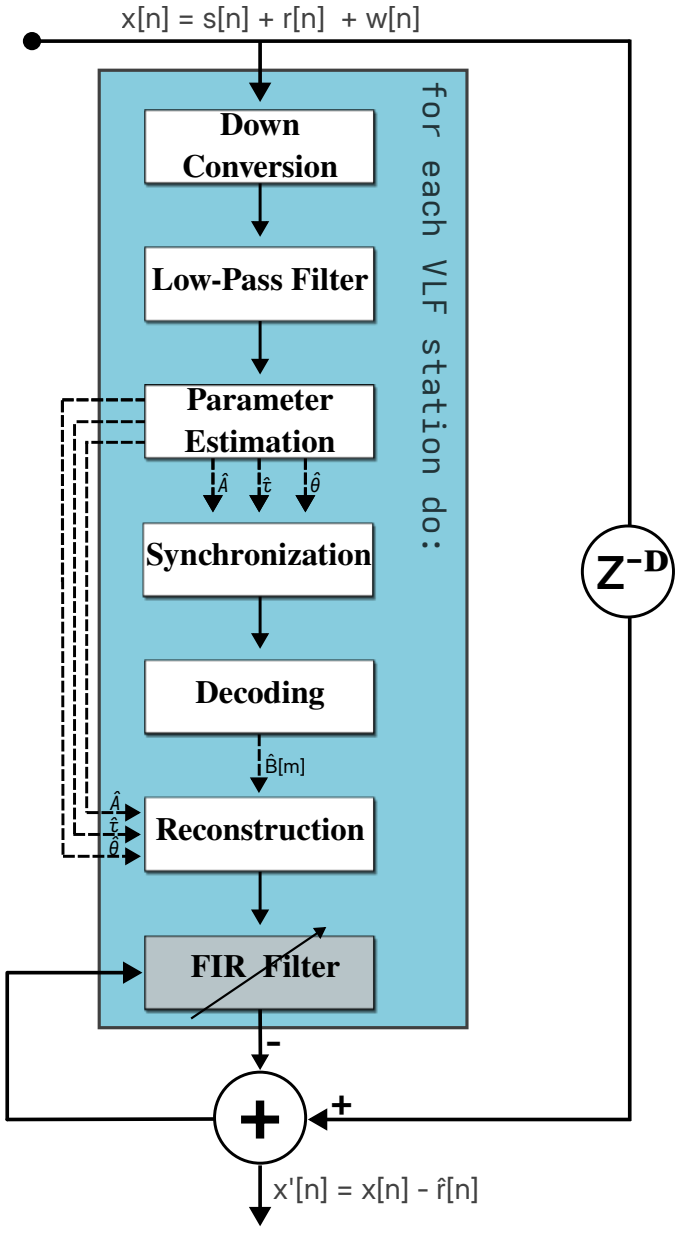

Figure 1. Block diagram of the model-and-subtract approach. The received signal $x[n]$ is composed of TEM signal $s[n]$, VLF radio noise, $r[n]$, and other noise, $w[n]$. Each VLF radio station is individually modeled and reconstructed. The reconstructed signal is fine-tuned with an adaptive FIR filter before subtraction. The z^{-D} block ensures the timing for the adaptive filter.

https://doi.org/10.5194/egusphere-2026-1141
Preprint. Discussion started: 25 March 2026

The estimated bit stream and signal parameters are used for reconstruction of a clean radio signal synchronous to the original noisy TEM signal. Ideally, this clean radio signal can be subtracted from the acquired data. However, due to inaccurate estimates of amplitude, symbol timing and phase, the clean radio signal is not perfectly matched to the noisy TEM signal. As a final step in the VLF/LF radio signal processing, we therefore pass the clean radio signal through an adaptive finite-impulse-response (FIR) filter, which fine-tunes the reconstructed signal for optimum noise removal. Since the clean radio signal is narrow band, a short adaptive filter with just a few taps is needed.

The adaptive FIR filter is based on the normalised-least-mean-square algorithm (Farhang-Boroujeny, 2013). It contains 25 taps and the normalized step size is 0.5 % of the maximum value. The adaptation of the filter is halted during the gaps in the data segment and in the early times of all segments where the zero values and the large TEM signal inflate the error and distort the adaptation.

3.2 Gating and stacking

The final step of TEM data processing is gating of data. We use semi-tapered gates with 50 % overlap (Larsen et al., 2021; Khare et al., 2024). The gates are composed of cosine-shaped rising and falling edges and a flat central section. The center time and gate width are exponentially increasing to produce ten gates per decade of time within the limits set by sampling rate and data record length.

After gating, mean values and standard errors of gate values are computed for plotting and analysis (Larsen et al., 2021). We also compute the covariance between the gate values. When TEM data contains noise from correlated sources, e.g., VLF radio signals, the correlated noise emerges as distinct, visible patterns in a plot of the associated covariance matrices and these matrices are therefore useful for algorithm comparison (McLachlan et al., 2023; Khare et al., 2024).

3.3 Synthetic noise

For assessing and comparing the performance of algorithms, data where the signal parameters and bit content of individual radio signals are known is necessary. For this purpose, we generate synthetic MSK-encoded radio signals using Eq. 1 with carrier frequencies and bit rates mimicking real VLF and LF radio stations (Rasmussen et al., 2018). For each radio signal, we draw a symbol timing between $-T_{sym}/2$ and $T_{sym}/2$ and signal phase between 0 and 2π from uniform distributions. The amplitudes of the radio signals are also randomly selected between 1 % and 10 % of the TEM signal amplitude. The different synthetic VLF and LF radio signals are summed. Further, white Gaussian noise is added to the signal accounting for the broadband thermal noise in real data. Our model does not take powerline noise or impulsive noise into consideration as these noise sources are adequately handled in standard processing steps. For the numerical experiments we use a 2 MHz sample rate.

https://doi.org/10.5194/egusphere-2026-1141
Preprint. Discussion started: 25 March 2026

3.4 Field noise

The field results presented below are based on the noisy-only data set used by Rasmussen et al. (2018). This data set was collected near Aarhus, Denmark using a multi-turn square coil with an effective area of 80.9 m^2. After amplification, the signal was continuously sampled for 25 s at a 500 kHz sample rate with a digital oscilloscope. To mimic TEM data, we introduce gaps into the data by setting sample values to zero in the data record corresponding to the transmitter pulse blinding.

3.5 TEM signal

A synthetic TEM signal decaying as $t^{-5/2}$ is added to each segment before processing. This smoothly decaying signal, which corresponds to the signal from a homogeneous half-space, captures the essential physics of a real TEM signal yet allows for easy visual inspection of sounding curves. The amplitudes of the TEM signals are chosen, so that the data in the first 5-10 gates have a high signal-to-noise ratio and the early decaying parts are clearly visible in all cases.

4 Results

4.1 The effect of gaps in data

The effect of gaps in data streams is investigated using synthetic data composed of known VLF/LF radio bit streams and white Gaussian noise. This allows us to quantify the bit error rate, which is an important factor in the model-and-subtract approach. Small errors in the estimates of, e.g., phase will lead to a slightly poorer result when a reconstructed VLF radio model is subtracted from data, but bit errors will lead to the subtraction of an outright wrong VLF radio model and consequently a very poor result.

The bit error rate is determined as a function of the gap length, i.e., the duration of transmitter pulses, while keeping the size of the subsequent data record containing the TEM transient signal fixed at 2048 μs. The gap length is varied over a range that includes typical low-moment pulses, 200 μs, and high-moment pulses, 450 μs, in common TEM instruments (Auken et al., 2019) and extends beyond the 5 ms duration of single bits in a 200 bit/s stream.

The results are plotted in Fig. 2. Each data point and the associated error bar (truncated at zero) are computed by repeating the numerical experiments 50 times. In each case a total bit error rate is computed for the four MSK radio stations in the model. A bit error rate of 0.0 corresponds to correct identification of all bits, a bit error rate of 1.0 corresponds to wrong identification of all bits, and a bit error rate of 0.5 corresponds to 50 % of all bits being correctly identified, like random guessing.

The results show that for all gap lengths up to 5 ms, the bit error rate remains very low and nearly flat. For gap lengths longer than 5 ms, the bit error rate increases significantly. These observation match the Viterbi decoder algorithm., i.e., the correlation between adjacent bits in the MSK bit stream ensures an efficient decoding even as the gap length approaches 5 ms. For gaps longer than 5 ms, this correlation is lost, which leads to the threshold seen in Fig. 2. Additional analysis of data sets with shorter or longer data records give similar results with longer records slightly improving performance. From this analysis we can conclude that the Viterbi algorithm is generally very efficient and if the gaps are less than 5 ms, bit errors are negligible.

https://doi.org/10.5194/egusphere-2026-1141
Preprint. Discussion started: 25 March 2026

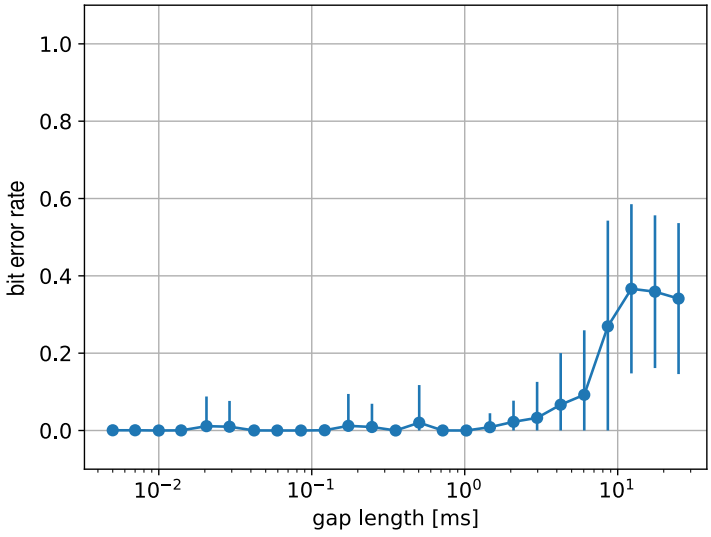

Figure 2. Bit error rate as a function of the gap length computed for a 2048 μs transient length. The lower part of the error bars are truncated at zero.

4.2 The effect of the adaptive filter

The effect of the adaptive filter in reconstruction of the VLF/LF radio signals in data with gaps is investigated through simulations where a synthetic signal composed of TEM data, interference from four MSK encoded radio signals, and white noise is processed in two manners. In the first case, the radio signals are reconstructed using the estimated amplitude, symbol timing, and symbol phase and subtracted from the data record. In the second case, an adaptive filter fine-tunes the VLF and LF radio signals before subtraction. In both cases we compute the mean square error as a function of the gap length, while keeping the size of the subsequent data record containing the TEM transient signal fixed at 2048 μs. The simulations are repeated 50 times for each gap length to compute mean values and standard deviations. With the chosen settings of the adaptive filter, it converges within about 0.5 ms. To improve signal quality, we cull the first segment where data are affected by the filter adaptation.

The results presented in Fig. 3 demonstrate that the adaptive filter significantly improves the results. The mean square error is reduced by more than an order of magnitude for all investigated gap lengths, and further, the standard deviation of the mean square error is reduced with the adaptive filter, which we ascribe to generally more accurate modeling in this case. Without the adaptive filter we observe a rise in the mean square error for long gap lengths above the 5 ms bit length, which corresponds with the increase in bit error rate, Fig. 2. Somewhat surprisingly, the adaptive filter performs well even in this limit. We ascribe this to the nonlinear filtering taking place in the adaptive algorithm, partially compensating for bit errors. From this analysis we can conclude that the algorithms for estimation of amplitude, symbol timing, and phase are generally quite accurate, but

https://doi.org/10.5194/egusphere-2026-1141
Preprint. Discussion started: 25 March 2026

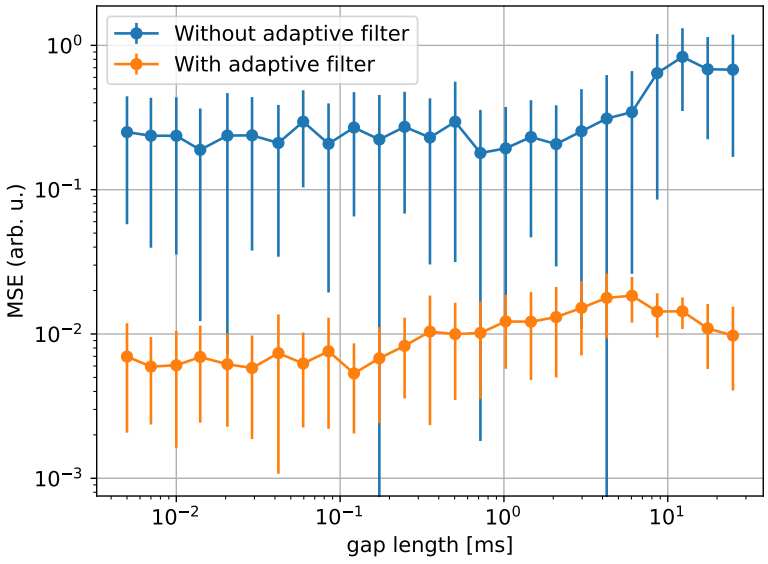

Figure 3. Mean square error after modeling and subtraction of VLF radio noise as a function of the transient length either with or without fine-tuning of the modeling with an adaptive filter.

that in a use-case like this where very high accuracy is needed for efficient noise removal, the performance can be significantly improved upon by automatic fine tuning with an adaptive filter.

4.3 Synthetic noise example

We demonstrate the benefits of the proposed approach using a sand-box example with synthetic VLF/LF radio noise, white Gaussian noise, and a simple TEM signal. The synthetic radio noise is composed of 4 radio signals at frequencies between 10 kHz and 80 kHz and operating at 100 bit/s or 200 bits/s. We construct data records composed of 500 transients interleaved with 200 μs gaps introduced into the model by zeroing out the corresponding intervals. The gaps occur at regular intervals matching an 817 Hz transmitter pulse repetition rate. The TEM signal is modeled as a simple half space with an easily identified $t^{-5/2}$ decay.

The synthetic data are processed in two manners. First, with a standard approach where the data are gated with semi-tapered gates and then stacked. Second, with the improved approach where the radio stations are first modeled and subtracted before the same gating and stacking is applied.

Plots of the stacked data and associated standard errors for the two processing methods are presented in Fig. 4. The corresponding covariance matrices are shown in Fig. 5.

In this idealized example, we see a very large improvement if VLF/LF radio interference is applied prior to gating and stacking. If the data are only gated and stacked, we start to see significant differences between the gated signal and the ideal

https://doi.org/10.5194/egusphere-2026-1141
Preprint. Discussion started: 25 March 2026

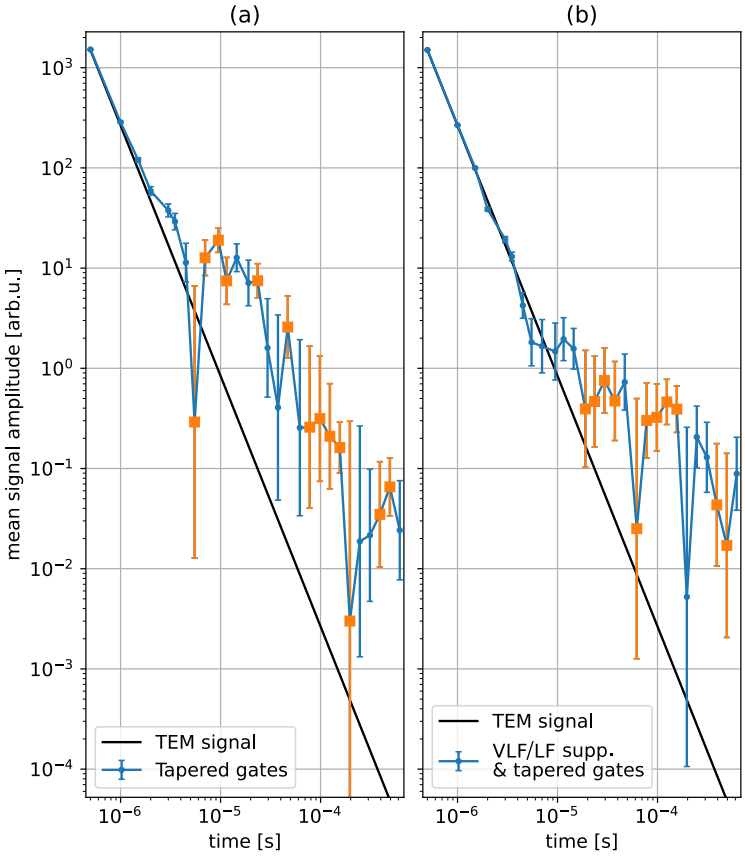

Figure 4. Sounding curve for a synthetic data example with a $t^{-5/2}$ TEM signal, four VLF/LF radio stations, and white Gaussian noise. Left: Semi-tapered gating and stacking. Right: Noise suppression with VLF/LF modeling and subtraction is applied prior to semi-tapered gating and stacking. Positive signal values are plotted in blue, negative signal values are sign-changed and plotted in orange.

$t^{-5/2}$ signal after about 3 μs, but by removing VLF/LF radio interference, significant differences do not occur until well after 10 μs. Further, the standard errors are much smaller when radio interference is removed. For a richer comparison, these observations are also quantified in Table 1 where gate values and standard errors are given for all odd-numbered gates. The table also gives the improvement in the standard errors computed as the ratio of the standard error with and without VLF/LF removal. This improvement ratio is much larger than unity until about gate 21 at around 125 μs. The reason for this behavior is that for early times, the VLF/LF radio interference for the four stations in the 10 kHz to 80 kHz range is located inside the frequency domain main-lobe of the semi-tapered gates and hence cannot be removed by gating. However, this restriction does not apply to the VLF/LF model and subtract approach. For late times, VLF/LF noise is located outside the main-lobe and the semi-tapered gates are efficiently removing the radio noise. Thus, there are no discernible differences between the two methods in this region.

https://doi.org/10.5194/egusphere-2026-1141
Preprint. Discussion started: 25 March 2026

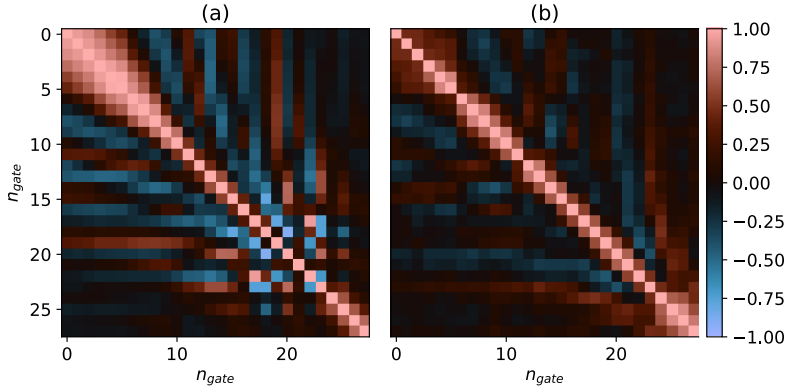

Figure 5. Covariance matrices for the synthetic data example with a $t^{-5/2}$ TEM signal, four VLF/LF radio stations, and white Gaussian noise.

Table 1. Gated TEM data (only odd gates are shown) for the case of a $t^{-5/2}$ TEM signal embedded in synthetic data noise composed of four VLF/LF radio stations and white noise. The last column gives the improvement in the standard error when VLF/LF processing is included.

Gate no.	Gate center [μs]	TEM (true)	TEM (without VLF/LF proc.)	TEM (with VLF/LF proc.)	SE improvement
1	0.0	1.500×10^{3}	$(1.529 \pm 0.007) \times 10^{3}$	$(1.502 \pm 0.001) \times 10^{3}$	5.06
3	1.0	9.622×10^{1}	$(12.42 \pm 0.757) \times 10^{1}$	$(9.826 \pm 0.164) \times 10^{1}$	4.63
5	2.5	1.701×10^{1}	$(3.558 \pm 0.781) \times 10^{1}$	$(2.006 \pm 0.135) \times 10^{1}$	5.76
7	4.0	6.173×10^{0}	$(2.722 \pm 7.995) \times 10^{0}$	$(6.233 \pm 0.952) \times 10^{0}$	8.40
9	6.5	2.045×10^{0}	$(-23.15 \pm 7.067) \times 10^{0}$	$(1.262 \pm 1.231) \times 10^{0}$	5.74
11	11.0	5.913×10^{-1}	$(-28.16 \pm 64.48) \times 10^{-1}$	$(-1.112 \pm 8.424) \times 10^{-1}$	7.65
13	18.5	1.685×10^{-1}	$(49.10 \pm 45.28) \times 10^{-1}$	$(12.80 \pm 6.00) \times 10^{-1}$	7.54
15	29.0	5.610×10^{-2}	$(375.2 \pm 254.5) \times 10^{-2}$	$(-4.73 \pm 52.45) \times 10^{-2}$	4.85
17	46.5	1.751×10^{-2}	$(-347.2 \pm 175.1) \times 10^{-2}$	$(-14.53 \pm 34.73) \times 10^{-2}$	5.04
19	77.5	4.935×10^{-3}	$(86.90 \pm 413.36) \times 10^{-3}$	$(94.38 \pm 109.11) \times 10^{-3}$	3.79
21	123.5	1.549×10^{-3}	$(54.72 \pm 56.55) \times 10^{-3}$	$(-32.61 \pm 53.72) \times 10^{-3}$	1.05
23	196.0	4.899×10^{-4}	$(1204 \pm 366) \times 10^{-4}$	$(1083 \pm 372) \times 10^{-4}$	0.98
25	311.0	1.548×10^{-4}	$(44.65 \pm 310.5) \times 10^{-4}$	$(165.4 \pm 317.6) \times 10^{-4}$	0.98
27	493.0	4.901×10^{-5}	$-1198 \times 10^{-5} \pm 2677 \times 10^{-5}$	$-1097 \times 10^{-5} \pm 2702 \times 10^{-5}$	0.99

The plot of covariance matrices in Fig. 5 show only small differences with or without modeling and subtraction of radio noise, even if there are large improvements in the standard errors of data. The reason for this is that the off-diagonal elements of the covariance matrices are scaled with the diagonal values before plotting and the scaling can therefore hide the improvement. This example is included to show that great care is needed in the interpretation of these covariance matrices.

https://doi.org/10.5194/egusphere-2026-1141
Preprint. Discussion started: 25 March 2026

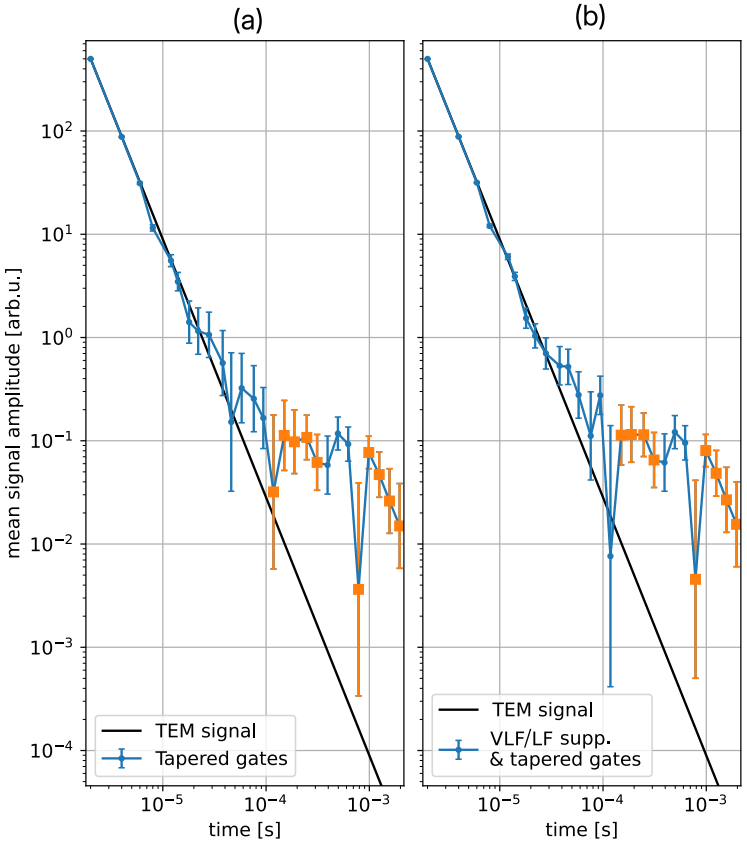

Figure 6. Sounding curve for an example with an artificial $t^{-5/2}$ TEM signal added to a noise-only data set recorded in the field. Left: Semi-tapered gating and stacking. Right: Noise suppression with VLF/LF modeling and subtraction is applied prior to semi-tapered gating and stacking. Positive signal values are plotted in blue, negative signal values are sign-changed and plotted in orange.

4.4 Field noise example

As a final validation of our approach, we utilize a noise-only data set with real VLF radio signals and other noise. As with the full synthetic example above, we embed a simple $t^{-5/2}$ TEM signal in the data as this allows for a clear visual interpretation and comparison of the results undisturbed by geological signatures in actual TEM data. The data are again processed either with gating and stacking or with modeling and subtraction of VLF and LF radio signals carried out prior to gating and stacking. The number of samples in a data record length is kept fixed, but due to a four times lower sample rate each transient is four times longer. The sounding curve is again obtained by stacking 500 transients.

The results are presented in Fig. 6 and Fig. 7, and the data for odd gates are summarized in Table 2. We observe the same trends in the field data example as in the synthetic data example, but the effects of VLF and LF removal are less pronounced in the sounding curve. This is expected as the field data also contains additional noise sources not found in the synthetic model.

https://doi.org/10.5194/egusphere-2026-1141
Preprint. Discussion started: 25 March 2026

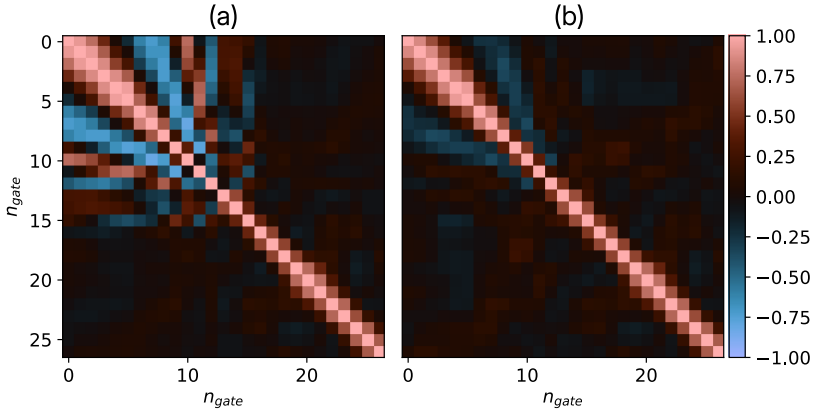

Figure 7. Covariance matrices for the noise-only field data set with an embedded artificial $t^{-5/2}$ TEM signal.

The best improvement is seen in the gates centered around 20 μs to 50 μs. The bandwidths of these gates are in the 20 kHz to 50 kHz range matching the main VLF radio signal components in the data set. For gates centered after about 100 μs, tapered gating is effective in suppressing radio noise and the results with or without modeling and subtraction of radio noise are almost identical.

In this field noise case, we see a dramatic improvement in the covariance matrix plot after removal of VLF and LF noise, Fig. 7. The structure in the off-diagonal elements seen up to about gate 15 is greatly reduced. We interpret this as the result of efficient suppression of the coherent radio noise.

The data presented in Table 2 completes the analysis. In the early gates, we see about two-fold improvement in the standard errors after removal of interfering radio signals. This improvement is smaller than observed for the synthetic case, which we ascribe to the simplified noise model. In the late gates where semi-tapered gating is effective, there are no differences in standard errors.

5 Discussion

The above results clearly demonstrate that even if time series contains regularly spaced gaps, the gaps can be handled, and bit streams can be efficiently decoded. Further, it was also demonstrated that the reconstruction of VLF and LF radio signals can be improved upon by including an adaptive filter to the signal processing chain. An important feature of this modeling and subtraction approach is that it only removes VLF and LF radio noise but does not distort the TEM signal of interest (Macnae, 2015; Rasmussen et al., 2018). This contrasts with advanced gating strategies where improved suppression of radio noise by gates designed to minimize the frequency response of side lobes will also affect the frequency response of the main lobe and potentially distort the TEM signal (Khare et al., 2024).

One known issue in VLF and LF radio modeling is sample rate mismatch, (Rasmussen et al., 2018). If the sampling frequency of the receiver is offset from the sampling frequency of the transmitter it will result in a small timing error that will accumulate

https://doi.org/10.5194/egusphere-2026-1141
Preprint. Discussion started: 25 March 2026

Table 2. Gated TEM data (only odd gates are shown) for the case of a $t^{-5/2}$ TEM signal embedded in real noise. The last column gives the improvement in the standard error when VLF and LF processing is included.

Gate no.	Gate center [μs]	TEM (true)	TEM (without VLF/LF proc.)	TEM (with VLF/LF proc.)	SE improvement
1	0	5.000×10^{2}	$(4.994\pm0.008)\times10^{2}$	$(4.996\pm0.004)\times10^{2}$	1.92
3	4	3.207×10^{1}	$(3.119\pm0.085)\times10^{1}$	$(3.163\pm0.046)\times10^{1}$	1.85
5	10	5.670×10^{0}	$(5.551\pm0.792)\times10^{0}$	$(6.051\pm0.389)\times10^{0}$	2.03
7	16	2.057×10^{0}	$(1.412\pm0.847)\times10^{0}$	$(1.538\pm0.385)\times10^{0}$	2.20
9	26	6.818×10^{-1}	$(10.616\pm6.990)\times10^{-1}$	$(7.011\pm2.909)\times10^{-1}$	2.40
11	44	1.971×10^{-1}	$(1.520\pm5.598)\times10^{-1}$	$(5.199\pm2.509)\times10^{-1}$	2.23
13	74	5.612×10^{-2}	$(25.55\pm27.86)\times10^{-2}$	$(11.14\pm18.65)\times10^{-2}$	1.49
15	116	1.870×10^{-2}	$(-3.200\pm14.607)\times10^{-2}$	$(0.762\pm13.262)\times10^{-2}$	1.10
17	186	5.837×10^{-3}	$(-97.67\pm100.6)\times10^{-3}$	$(-115.0\pm98.97)\times10^{-3}$	1.02
19	310	1.644×10^{-3}	$(-61.73\pm53.29)\times10^{-3}$	$(-65.13\pm55.14)\times10^{-3}$	0.97
21	494	5.162×10^{-4}	$(1175\pm523)\times10^{-4}$	$(1212\pm542)\times10^{-4}$	0.96
23	784	1.633×10^{-4}	$(-36.38\pm355.4)\times10^{-4}$	$(-45.53\pm368.5)\times10^{-4}$	0.96
25	1244	5.161×10^{-5}	$(-4705\pm3108)\times10^{-5}$	$(4840\pm3221)\times10^{-5}$	0.96
27	1962	1.655×10^{-5}	$(-1496\pm2358)\times10^{-5}$	$(-1551\pm2440)\times10^{-5}$	0.97

over time. If this timing error is small enough it will be mitigated by the adaptive filter. Another important aspect of the adaptive filter is that it will automatically adapt to small changes in the received signal caused by, e.g., slow changes in the atmosphere / signal path from the radio station to the TEM instrument.

The model-and-subtract approach present here is based on a combination of prior knowledge and handheld processing. For the case of the synthetic model, the frequencies and bit rates of radio stations were preselected and for the case of field noise data, the frequencies and bit rates were known from prior work and public data, and the processing made use of these known values (Rasmussen et al., 2018). In future applications of this approach, it will be beneficial with robust, automated algorithms, with little or no user interference. One potential solution for this is compiling an extensive list of known MSK-encoded VLF and LF radio stations with their associated center frequencies and bit rates. Analysis of a noise-only segment of data recorded prior to the TEM data collection can reveal what radio sources are active and if the amplitudes of these are significant enough to make modeling and subtraction worthwhile.

In this work we have only focused on VLF and LF radio signals encoded with minimum-shift keying. However, this is not the only type of radio interference found in TEM data. One example of this is the German DCF77 radio station (WikiPedia, 2025), which transmits a time synchronization signal at 77.5 kHz, which can be detected throughout most of Europe and is also present in our data. This radio station employs a well-documented combined amplitude modulation and phase modulation

https://doi.org/10.5194/egusphere-2026-1141
Preprint. Discussion started: 25 March 2026

format. Removal of the interference from DCF77 should therefore also be possible by a similar reconstruction of this radio signal.

We have presented an offline implementation of our method. However, it appears feasible to design and implement the algorithms in real time for roving TEM data collection where data sampled at MHz rates are normally gated on-the-fly to avoid storage of excessive amounts of data. Such algorithms would likely be designed in a block-based manner where the typically several hundred transients that go into a sounding curve are treated as one block and processed collectively. The computational requirements for the algorithm are modest and the looping over the different VLF and LF radio stations can be parallelized.

6 Conclusions

It is well established that modeling and subtraction of MSK-encoded VLF and LF radio signals is an efficient method for handling this ubiquitous noise in TEM data. In this paper, we have explored the scenario, where the TEM data stream is interrupted by regularly spaced gaps, which is inherent to new time-lapse applications of TEM. Even in this case, the algorithms work efficiently, under the constraint that gaps are kept short enough, i.e., enough data are available between gaps. The reconstruction of the radio interference was found to be significantly improved upon by including an adaptive filter for fine tuning of amplitude, timing, and phase. For the case of a field noise data set we showed that modeling and subtraction of VLF and LF radio interference improved the standard error of the TEM signal by about a factor of two. Such an improvement will be important for constraining inversion results in future uses of the method.

Data availability. The data used for figures 6 and 7 are availble in Larsen (2026).

Author contributions. MH: Algorithm and software development, data analysis. JJL: conceptualization, project management, data analysis, and manuscript writing.

Competing interests. The authors declare that they have no conflict of interest.

Acknowledgements. This work is supported by Innovation Fund Denmark through the SuperTEM project, 0177-00085A. Pradip Kumar Maurya, Nikolaj Foged, Smith K. Khare, Claes Eske Harbo Jensen, and Kranti Kamble are kindly acknowledged for discussions.

https://doi.org/10.5194/egusphere-2026-1141
Preprint. Discussion started: 25 March 2026

References

Asif, M. R., Maurya, P. K., Foged, N., Larsen, J. J., Auken, E., and Christiansen, A. V.: Automated Transient Electromagnetic Data Processing for Ground-Based and Airborne Systems by a Deep Learning Expert System, IEEE Transactions on Geoscience and Remote Sensing, 60, 5919 814, https://doi.org/10.1109/TGRS.2022.3202304, 2022.

Auken, E., Foged, N., Larsen, J. J., Lassen, K. V. T., Maurya, P. K., Dath, S. M., and Eiskjær, T. T.: tTEM - A towed transient electromagnetic system for detailed 3D imaging of the top 70 m of the subsurface, GEOPHYSICS, 84, E13–E22, https://doi.org/10.1190/geo2018-0355.1, 2019.

Behroozmand, A. A., Auken, E., and Knight, R.: Assessment of Managed Aquifer Recharge Sites Using a New Geophysical Imaging Method, Vadose Zone Journal, 18, 1–13, https://doi.org/10.2136/vzj2018.10.0184, 2019.

Chandra, S., Auken, E., Maurya, P. K., Ahmed, S., and Verma, S. K.: Large Scale Mapping of Fractures and Groundwater Pathways in Crystalline Hardrock By AEM, Scientific Reports, 9, 398, https://doi.org/10.1038/s41598-018-36153-1, 2019.

Chen, K., Zhang, J., Xue, G., Huang, H., Chen, W., Hao, J., and Yue, Y.: Feasibility of Monitoring Hydraulic Connections between Aquifers Using Time-lapse TEM: A Case History in IInner Mongolia, China, Journal of Environmental and Engineering Geophysics, 24, 361–372, https://doi.org/10.2113/JEEG24.3.361, 2019.

Engebretsen, K. W., Zhang, B., Fiandaca, G., Madsen, L. M., Auken, E., and Christiansen, A. V.: Accelerated 2.5-D inversion of airborne transient electromagnetic data using reduced 3-D meshing, Geophysical Journal International, 230, 643–653, https://doi.org/10.1093/gji/ggac077, 2022.

Eppelbaum, L. V.: VLF-method of geophysical prospecting: A non-conventional system of processing and interpretation (implementation in the Caucasian ore deposits), ANAS Transactions, Earth Sciences, 2, 16–38, https://doi.org/10.33677/ggianas20210200060, 2021.

Farhang-Boroujeny, B.: Adaptive Filters – Theory and Applications, Wiley, 2. edn., 2013.

Gisselø, P., Daoultzis, P., and Smart, E.: Deep Targeting With Airborne Electromagnetic Surveys, in: NSG2024, 4th Conference on Airborne, Drone and Robotic Geophysics, pp. 1–5, Helsinki, Finland, https://doi.org/10.3997/2214-4609.202420190, 2024.

Hördt, A., Andrieux, P., Neubauer, F. M., Rüter, and Vozoff, K.: A first attempt at monitoring underground gas storage by means of time-lapse multichannel transient electromagnetics, Geophysical Prospecting, 48, 489–509, https://doi.org/10.1046/j.1365-2478.2000.00192.x, 2000.

Khare, S. K., McLachlan, P., Maurya, P. K., and Larsen, J. J.: An optimized and hybrid gating scheme for the suppression of very low-frequency radios in transient electromagnetic systems, Geoscientific Instrumentation, Methods and Data System, 13, 27–41, https://doi.org/10.5194/gi-13-27-2024, 2024.

Larsen, J. J.: VLF Modelling, [Dataset]. Zenodo, 10.5281/zenodo.19051738, 2026.

Larsen, J. J., Pedersen, S. S., Foged, N., and Auken, E.: Suppression of very low frequency radio noise in transient electromagnetic data with semi-tapered gates, Geoscientific Instrumentation, Methods and Data Systems, 10, 81–90, https://doi.org/10.5194/gi-10-81-2021, 2021.

Lysdahl, A. K., Christensen, C. W., Pfaffhuber, A. A., Vöge, M., Andresen, L., Skurdal, G. H., and Panzner, M.: Integrated bedrock model combining airborne geophysics and sparse drillings based on an artificial neural network, Engineering Geology, 297, 106 484, https://doi.org/10.1016/j.enggeo.2021.106484, 2022.

Macnae, J.: Stripping very low frequency communication signals with minimum shift keying encoding from streamed time-domain electromagnetic data, Geophysics, 80, E343–E353, https://doi.org/10.1190/geo2015-0304.1, 2015.

https://doi.org/10.5194/egusphere-2026-1141
Preprint. Discussion started: 25 March 2026

Macnae, J. C., Lamontagne, Y., and West, G. F.: Noise processing techniques for time-domain EM systems, GEOPHYSICS, 49, 934–948, https://doi.org/10.1190/1.1441739, 1984.

McLachlan, P., Christensen, N. B., Grombacher, D., and Christiansen, A. V.: Evaluating the impact of correlated noise for time-lapse transient electromagnetic (TEM) monitoring studies, Near Surface Geophysics, 21, 333–342, https://doi.org/10.1002/nsg.12262, 2023.

Morelli, M. and Vitetta, G.: Joint phase and timing synchronization algorithms for MSK-type signals, in: 1999 IEEE Communications Theory Mini-Conference (Cat. No.99EX352), pp. 146–150, https://doi.org/10.1109/CTMC.1999.790254, 1999.

Nabighian, M. N. and Macnae, J. C.: 6. Time Domain Electromagnetic Prospecting Methods, in: Electromagnetic Methods in Applied Geophysics: Volume 2, Application, Parts A and B, chap. 6, pp. 427–520, SEG Library, https://doi.org/10.1190/1.9781560802686.ch6, 1991.

Peng, C., Zhu, K., Fan, T., and Yang, Y.: Suppressing the very low-frequency noise by B-spline gating of transient electromagnetic data, Journal of Geophysics and Engineering, 19, 761–774, https://doi.org/10.1093/jge/gxac049, 2022.

Qi, Z., Li, X., Li, H., and Liu, W.: First Results From Drone-Based Transient Electromagnetic Survey to Map and Detect Unexploded Ordnance, IEEE Geoscience and Remote Sensing Letters, 17, 2055–2059, https://doi.org/10.1109/LGRS.2019.2962754, 2020.

Rasmussen, S., Nyboe, N. S., Mai, S., and Larsen, J. J.: Robust cancellation of minimum shift keying-encoded radio interference in data from the transient electromagnetic method, Geophysics, 83, E87–E94, https://doi.org/10.1190/geo2017-0611.1, 2018.

Swidinsky, A. and El-Kaliouby, H.: Time-lapse transient electromagnetic monitoring of a water infiltration experiment: An application to the Central Avra Valley recharge basin, Tucson, Arizona, in: SEG Technical Program Expanded Abstracts, pp. 4439–4443, https://doi.org/10.1190/segam2013-0331.1, 2013.

WikiPedia: DCF77, https://en.wikipedia.org/wiki/DCF77, accessed: 2025-06-19, 2025.

With, C., Löfroth, H., Bastani, M., Persson, L., Rodhe, L., and Hedfors, J. Schoning, K.: A methodology for mapping of quick clay in Sweden, Natural Hazards, 112, 2549–2576, https://doi.org/10.1007/s11069-022-05278-y, 2022.

Wu, S., Huang, Q., and Zhao, L.: A deep learning-based network for the simulation of airborne electromagnetic responses, Geophysical Journal International, 233, 253–263, https://doi.org/10.1093/gji/ggac463, 2022.

Zamora-Luria, J. C., McLachlan, P., Maurya, P. K., Liu, L., Grombacher, D., and Christiansen, A. V.: A feasibility study on time-lapse transient electromagnetics for monitoring groundwater dynamics, Geophysics, 88, E135–E146, https://doi.org/10.1190/GEO2022-0532.1, 2023.